

Article citation info:

Su C, Chen H, Wen Z. Prediction of remaining useful life for lithium-ion battery with multiple health indicators. *Eksploracja i Niezawodność – Maintenance and Reliability* 2021; 23 (1): 176–183, <http://dx.doi.org/10.17531/ein.2021.1.18>.

Prediction of remaining useful life for lithium-ion battery with multiple health indicators

Chun Su^{a, b, *}, Hongjing Chen^a, Zejun Wen^b

^aSchool of Mechanical Engineering, Southeast University, Nanjing 211189, China

^bHunan Provincial Key Lab of Health Maintenance for Mechanical Equipment, Hunan University of Science and Technology, Xiangtan 411201, Hunan, China

Indexed by:



Highlights

- Four types of health indicators (HIs) are built with the battery operating data.
- GRNN is applied to estimate the battery's remaining capacity with the HIs.
- Based on the predicted capacity value, the battery's RUL is estimated with NAR.

Abstract

Lithium-ion (Li-ion) battery has become a primary energy form for a variety of engineering equipments. To ensure the equipments' reliability, it is crucial to accurately predict Li-ion battery's remaining capacity as well as its remaining useful life (RUL). In this study, we propose a novel method for Li-ion battery's online RUL prediction, which is based on multiple health indicators (HIs) and can be derived from the battery's historical operation data. Firstly, four types of indirect HIs are built according to the battery's operation current, voltage and temperature data respectively. On this basis, a generalized regression neural network (GRNN) is presented to estimate the battery's remaining capacity, and the non-linear autoregressive approach (NAR) is applied to predict the battery's RUL based on the estimated capacity value. Furthermore, to reduce the interference, twice wavelet denoising are performed with different thresholds. A case study is conducted with a NASA battery dataset to demonstrate the effectiveness of the method. The result shows that the proposed method can obtain Li-ion batteries' RUL effectively.

Keywords

This is an open access article under the CC BY license (<https://creativecommons.org/licenses/by/4.0/>)

lithium-ion (Li-ion) battery, remaining useful life (RUL), health indicator (HI), generalized regression neural network (GRNN), non-linear autoregressive (NAR).

1. Introduction

Lithium-ion (Li-ion) battery is the key power unit for a variety of engineering equipments, including portable computers, electric automobiles, satellites, and spacecrafts, etc. With the increased cycles of charge-discharge, the battery's capacity will deteriorate gradually, and when the capacity is inferior to a given threshold, failure may occur. This phenomenon will reduce the equipment's reliability and even lead to catastrophic failures [31]. Therefore, it is crucial to timely forecast Li-ion battery's capacity as well as its remaining useful life (RUL).

For Li-ion battery, its RUL can be defined as the number of remaining charge-discharge cycles before the battery's capacity deteriorates to a predetermined failure threshold [1]. The prediction methods for battery RUL can be categorized into three types, i.e. model-based approach, data-driven approach and hybrid approach [23]. Model-based approaches adopt mathematical representation or failure physics model to describe the degradation process of battery capacity, including electrochemical model [14, 16, 25], equivalent circuit model [6] and empirical model [33], etc. Considering the interactions among the various factors and the calculation of the parameters, it is not easy to establish a reliable and accurate prediction model for the electrochemical model and equivalent circuit model. Conversely, by fitting

a large amount of degradation data, empirical model is easier to be established [32].

Based on the battery's historical operational data, data-driven approach can extract the feature information and obtain the inherent degradation tendency. As a kind of data-driven approach, time series analysis has been widely used in RUL prediction, including autoregressive (AR) [12], autoregressive and moving average (ARMA) [18], autoregressive integrated moving average (ARIMA) [39] and the improved models [13, 35]. In recent years, artificial intelligence (AI) algorithm becomes a hot point in data-driven approaches due to its powerful ability in self-learning and data mining. The frequently-used AI algorithms include artificial neural network (ANN) [11, 21, 30], support vector machine (SVM) [15, 26], relevance vector machine (RVM) [36], etc.

By combining two or more model-based or data-driven approaches, hybrid approach can overcome the limitations of a single method and thus improve the accuracy and efficiency of the prediction [5, 37]. Hybrid approach can be a combination of model-based approach and data-driven approach, and it can also be a combination of two or more types of data-driven approaches [1, 22].

In most existing studies, the Li-ion battery's RUL is predicted with static capacity data. In fact, the battery's remaining capacity can only be measured when it is out of service, meanwhile it also requires strict

(*) Corresponding author.

E-mail addresses: C. Su - suchun@seu.edu.cn, H. Chen - s820086099@163.com, Z. Wen - zjwen732@163.com

testing conditions and environment. Therefore, it is difficult to be applied in engineering practice. To solve this problem, some other discriminant criteria can be used to estimate the battery's remaining capacity as well as its RUL, e.g. internal resistance [9, 10], incremental capacity analysis (ICA) [27, 28], open circuit voltage (OCV), entropy [2, 7, 29], etc [34]. Here, we call them the health indicators (HIs).

In this study, on the basis of battery's operation data, a novel hybrid approach is proposed for estimating Li-ion battery RUL, and multiple HIs are adopted concurrently. Generally, there are three steps in it. Fig. 1 is the flowchart of the proposed method.

Step 1: Calculating HIs. Based on the data, including battery's current, voltage and working temperature, four types of HIs are built accordingly. They are calculated resistance (CR), rate of temperature change (TR), duration time of equal discharging voltage difference (DTEDVD) and sample entropy of discharge voltage (SampEn), respectively.

Step 2: Estimating the remaining capacity. A generalized regression neural network (GRNN) with cross-validation is applied to estimate the battery's remaining capacity. To reduce the interference and improve the accuracy of the estimation, the wavelet denoising is performed for two times and with different thresholds.

Step 3: Predicting RUL. With the estimated remaining capacity, the battery's RUL is predicted via the non-linear autoregressive (NAR) method.

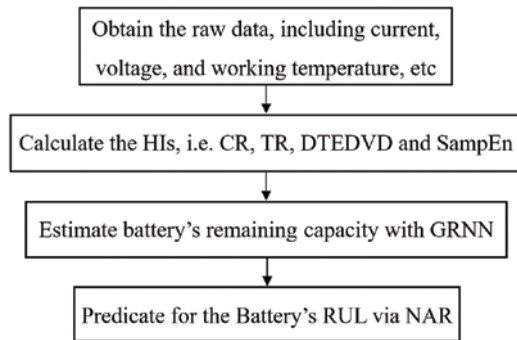


Fig. 1. Process of the proposed approach

The remainder of this article is organized as follows. Section 2 introduces the four HIs and their calculation methods respectively. Section 3 illustrates the basic theory of GRNN, NAR and wavelet denoising. Based on the Li-ion battery data from NASA, Section 4 conducts a case study of Li-ion battery RUL prediction, and the effectiveness of the proposed approach is illustrated. Conclusions and future works are given in Section 5.

2. Health indicators

To illustrate the discharging characteristics of the battery changing with the number of the charge cycles, in this study four HIs are extracted, they are CR, TR, DTEDVD and SampEn respectively. The value of the above four HIs will change with the increase of cycles, and the corresponding calculation methods are described as the follows.

2.1. Calculation of CR

For Li-ion battery, its internal resistance is closely related to the battery's remaining capacity. Saha et al [19] found that the remaining capacity of Li-ion batteries is linearly related to the sum of their electrolyte impedance and the charge transfer impedance.

CR is the measured internal resistance, which can be obtained with battery's terminal voltage and current during its operating state. Fig. 2 depicts the voltage and current's change at the instant of battery discharge. When a constant DC current passes through the battery, the terminal voltage changes ΔU_n at the time t_1 . At that time, the polariza-

tion effect has not occurred in the battery, therefore the voltage change is caused by ohm resistance. In this paper, the CR refers to the ohmic resistance R_n . According to Ohm's Law, it can be obtained as [18]:

$$R_n = \frac{\Delta U_n}{I_n} \quad n = 1, 2, \dots, N \quad (1)$$

where ΔU_n is the voltage change caused by ohmic resistance of cycle n ; I_n is the load current in cycle n ; and N is the total cycle life of the battery.

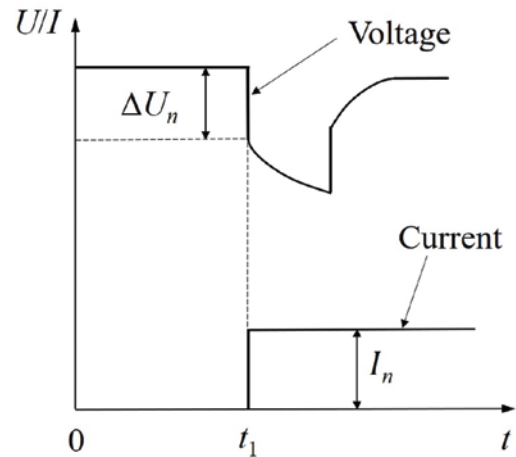


Fig. 2. Pulse discharge response of the battery

2.2. Calculation of TR

During the discharging process, the battery's internal temperature will change. Here we define TR as the rate that the temperature changes in the discharge process. TR will increase with the increase of cycles. In cycle n , TR can be calculated as follows:

$$TR_n = (TP_e^n - TP_s^n) / t_n \quad n = 1, 2, \dots, N \quad (2)$$

where TR_n denotes the rate of temperature change in cycle n ; TP_e^n is the end temperature of cycle n ; TP_s^n is the initial temperature of cycle n ; and t_n is the duration time of cycle n 's discharge process.

2.3. Calculation of DTEDVD

For Li-ion battery, the time for full discharge will be shortened gradually with the increase of the cycles. Therefore, the duration time of equal discharging voltage difference (DTEDVD) will also be shortened with the increase of the cycles' number. For a constant voltage interval $[U_L, U_H]$. We define t_D^n as the duration time in cycle n when the voltage is reduced from U_H to U_L , as shown in Fig. 3.

$$t_D^n = |t_H^n - t_L^n| \quad n = 1, 2, \dots, N \quad (3)$$

where t_D^n denotes the duration time of equal discharging voltage difference in cycle n ; t_H^n denotes the moment that the discharge voltage is U_H in cycle n ; and t_L^n denotes the moment that the discharge voltage is U_L in cycle n .

2.4. Calculation of SampEn

Sample entropy (SampEn) was firstly proposed by Richman and Moorman to measure the complexity of time series [17]. In this study, we regard the discharging process as a time series, and the SampEn of discharge voltage is used as an HI for the Li-ion battery.

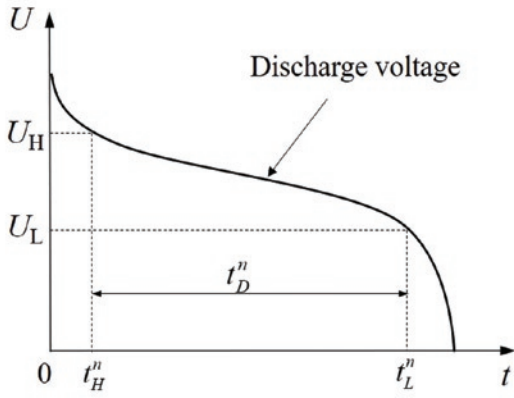


Fig. 3. Duration time of equal discharging voltage difference

For a given embedding dimension m , tolerance r as well as the number of data point T , we can obtain a time-series data set $X = \{x_1, x_2, x_3, \dots, x_T\}$ with a constant time interval τ . Here we define a template vector of length m , $X_m(\alpha) = [x(\alpha), x(\alpha+1), \dots, x(\alpha+m-1)]$ $\alpha = 1, 2, \dots, T-m+1$. The distance between two template vectors of $X_m(\alpha)$ and $X_m(\beta)$ is define as $d_m[X_m(\alpha), X_m(\beta)]$ ($\alpha \neq \beta$). It can be any types of distance functions, including Euclidean distance, or Chebyshev distance.

$V^m(\alpha)$ is defined as the number of $d_m[X_m(\alpha), X_m(\beta)] \leq r$ ($\alpha \neq \beta$), and the definition of the function is as the follows [28]:

$$B_\alpha^m(r) = \frac{1}{T-m+1} V^m(\alpha) \quad \alpha = 1, 2, \dots, T-m+1 \quad (4)$$

$$B^m(r) = \frac{1}{T-m} \sum_{\alpha=1}^{T-m} B_\alpha^m(r) \quad (5)$$

where $B^m(r)$ represents the probability that two sequences will match for m points. Similarly, we can obtain $B^{m+1}(r)$. Hence, the sample entropy can be defined as:

$$SampEn(r, m, T) = -\ln \left[\frac{B^{m+1}(r)}{B^m(r)} \right] \quad (6)$$

3. Methodology

In this study, the battery's remaining capacity is estimated with the proposed HIs. On this basis, by analyzing the degradation trend of the remaining capacity, the battery's RUL is predicted.

GRNN is used to establish the mapping relationship between the HIs and the battery's capacity, and hereafter to estimate the remaining capacity. Here, NAR model is used to demonstrate the degeneration of battery capacity. Moreover, wavelet denoising is applied to reduce the interference of the estimated capacity. Here, we illustrate the basic theories for GRNN, NAR and wavelet denoising as the follows.

3.1. Theory of GRNN

With a flexible network structure, GRNN model has strong ability for non-linear mapping. Therefore, it is suitable for solving non-linear problems [38].

Generally, there are four layers in GRNN, i.e. input layer, pattern layer, summation layer, and output layer, as shown in Fig. 4. The input of the network is $\mathbf{X} = [x_1, x_2, \dots, x_e]^T$, and its output is

$\mathbf{Y} = [y_1, y_2, \dots, y_k]^T$. d is the dimension of the input vector, k is the dimension of the output sample, and m is the number of the learning sample.

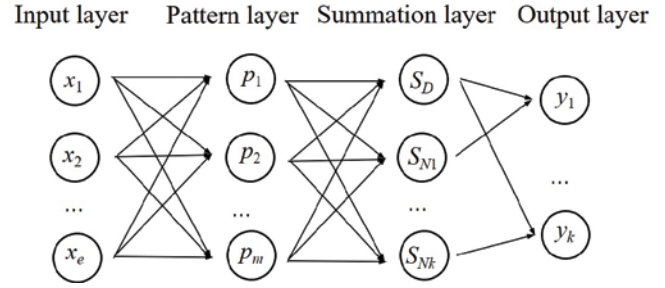


Fig. 4. Basic structure of the GRNN

- (1) Input layer: Among it, each neuron is a simple distribution unit, which will transfer the input variable directly to the pattern layer. In addition, the number of the input neurons in a GRNN equals to the dimension of the input vector e .
- (2) Pattern layer: The number of neurons equals to the number of learning sample m . Each neuron corresponds to a different sample, and the neurons transfer function can be calculated as [36]:

$$p_i = \exp \left[-\frac{(\mathbf{X} - \mathbf{X}_i)^T (\mathbf{X} - \mathbf{X}_i)}{2\sigma^2} \right] \quad i = 1, 2, \dots, m \quad (7)$$

where σ is the smoothing parameter; \mathbf{X} is the input variable; and \mathbf{X}_i is the corresponding learning sample of neuron i .

- (3) Summation layer: It sums the output of the pattern layer. In this layer, two types of neurons are used for summation. The simple summation of the pattern outputs is determined with:

$$S_D = \sum_{i=1}^m p_i \quad (8)$$

And, the weighted summation of the pattern output can be determined by:

$$S_{Nj} = \sum_{i=1}^m y_{ij} p_i \quad j = 1, 2, \dots, k \quad (9)$$

where y_{ij} is the weight of the i -th neuron in the pattern layer, which is connected to the summation layer.

- (4) Output layer: The results calculated in the summation layer will be sent to the output layer. The number of neurons is equal to the dimension k of the output vector in the sample. The output of the neurons is calculated as follows:

$$y_j = \frac{S_{Nj}}{S_D} \quad j = 1, 2, \dots, k \quad (10)$$

where y_j is the output of the j -th node in the output layer.

In this study, the cross-validation is used to gain the optimized parameters.

3.2. Theory of NAR

Here, by combining the variable's information during the early time, NAR model is used to describe the variable information at a particular time. It is a form of time series [8]:

$$y(t) = f[y(t-1), y(t-2), \dots, y(t-p)] \quad (11)$$

where p is the delay time, namely the order of the neural network (NN); and $f(\cdot)$ is the model of NAR.

The structure of NAR-NN is shown as in Fig. 5. It is consisted of four layers, i.e. input layer, hidden layer, output layer and the delay function.

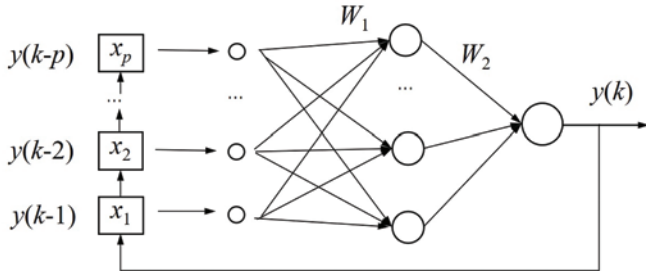


Fig. 5. Structure of NAR-NN

In Fig.5, x_u ($1 \leq u \leq p$) is the input; $y(k)$ is the output; W_1 is the connection weight between the input layer and the hidden layer; W_2 is the connection weight between the hidden layer and the output layer; and p is the delay time of the output.

The output of the node v in the hidden layer is:

$$h_v = g_1 \left(\sum_{u=1}^p w_{uv} x_u + c_v \right) \quad v = 1, 2, \dots, V \quad (12)$$

where $g_1(\cdot)$ is the activation function of the hidden nodes; V is the number of the hidden nodes; x_u is the u -th delay output of the output signal y ; w_{uv} is the connection weight between the hidden node u and the delay node v ; and c_v is the v -th neural threshold of the hidden layer.

The output of NAR is:

$$y = g_2 \left(\sum_{v=1}^V w_v h_v + d \right) \quad (13)$$

where w_v is the connection weight between the hidden node v and the output node; and d is the neural threshold of the output layer.

3.3. Wavelet denoising

Wavelet analysis is a kind of method for signal analysis, which can separate the noise signals and extract effective data from the noise-mixed data. In wavelet analysis, the data can be decomposed into two parts with the expansion and translation of the mother wavelet, i.e. approximate part and detail part [24].

Let $H(x)$ denote the measured signal mixed with noise, the wavelet transform with the mother wavelet $\psi(x)$ can be expressed as:

$$c(a, b) = \langle H(x), \psi_{a,b}(x) \rangle = \frac{1}{\sqrt{|a|}} \int_{-\infty}^{+\infty} H(x) \psi \left(\frac{x-b}{a} \right) \quad (14)$$

where a and b are the expansion and translation parameters of the mother wavelet respectively; and $c(a, b)$ is the wavelet coefficient of $H(x)$.

During the process of wavelet denoising, the selection of wavelet denoising threshold is closely related to the consequence of noise reduction. In this study, a twice denoising method with different thresh-

olds is applied [3, 4]. The first denoising threshold is made by the Sqtwolog method:

$$\lambda_{sqt} = \sqrt{2 \log N} \quad (15)$$

And, the second denoising threshold is finished by the minimax method:

$$\lambda_{\min} = 0.3936 + 0.1829 \log_2^N \quad (16)$$

where N is the number of signal $H(x)$. In this paper, it equals to the cycle life of the battery.

The thresholds of the above two methods are usually different, and the threshold of the Sqtwolog method is larger than that of the minimax method. Therefore, the first wavelet denoising can remove the larger noise signal, while the second wavelet denoising can remove the smaller noise signal. By using the twice wavelet denoising with different thresholds, the interference among the measured data can be reduced effectively.

3.4. Implementation of the proposed approach

Here, the training batteries are used to establish the mapping relationship between the HIs and the battery capacity. The basic steps for estimating battery RUL are described as follows:

- (1) Based on the historical operation data, the HIs of the training batteries and testing batteries are calculated respectively.
- (2) By using the training batteries, train a GRNN model to establish the mapping relationship between the HIs and the battery's capacity.
- (3) With the HIs data of testing batteries in the previous cycles, the capacity of the testing batteries is estimated on the basis of the well-trained GRNN model.
- (4) The wavelet denoising is applied to deduce the noising of the estimated capacity.
- (5) With the established capacity sequence and by using the NAR model, the remaining capacity and RUL of the testing battery can be predicted.

4. Prognostics Experiment

4.1. Experiment Data and the Procedure

In this section, a case study is conducted to demonstrate the effectiveness and efficiency of the proposed approach, where the Li-ion battery data come from the data repository of the NASA Ames Prognostics Center of Excellence (PCoE) [20]. Here, three groups of batteries are taken as examples, i.e. B05, B06 and B07. Among them, B05 and B06 are used as the training batteries, and B07 is used as the target battery. The experimental parameters of the discharge process are listed as in Table 1.

Table 1. Discharging parameters of the NASA batteries

Battery No.	$T/^\circ\text{C}$	I_{dis}/A	V_{up}/V	V_{low}/V	C_{new}/Ah
B05	24	2	4.2	2.7	1.86
B06	24	2	4.2	2.5	2.04
B07	24	2	4.2	2.2	1.89

The capacity's degradation trends with the cycles are shown as in Fig. 6. Obviously, the battery's capacity shows a non-monotonic decline with the increase of the cycles. Meanwhile, the degradation is accompanied with the phenomena of capacity self-regeneration as

well as local fluctuations. Therefore, it is essential to develop an effective prognostic approach to accurately estimate the capacity and predict its RUL by overcoming the uncertainty fluctuation.

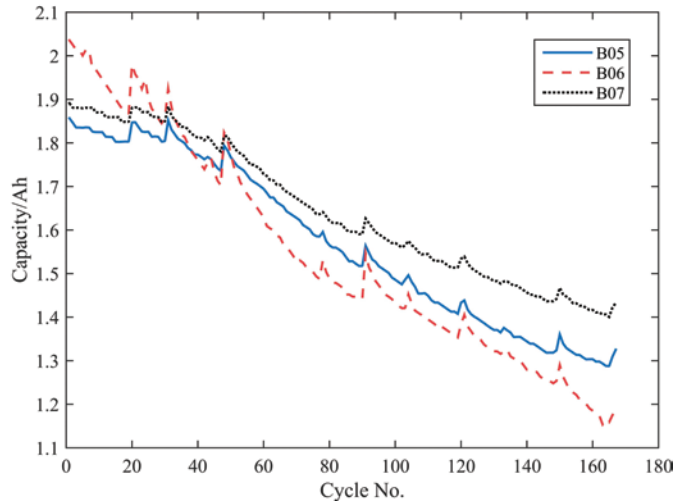
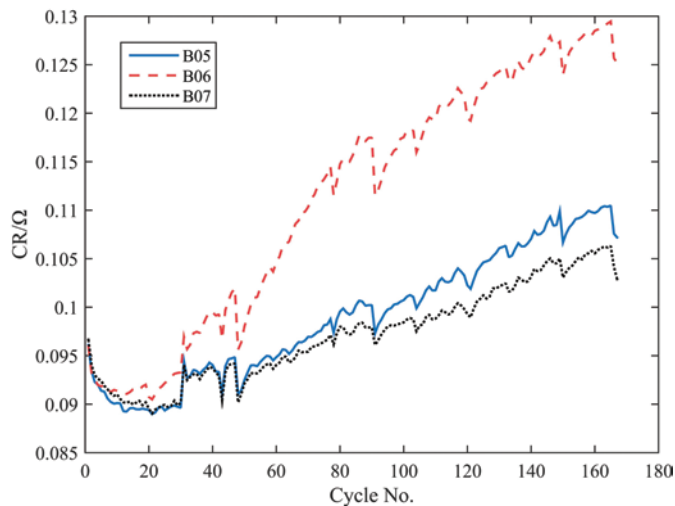
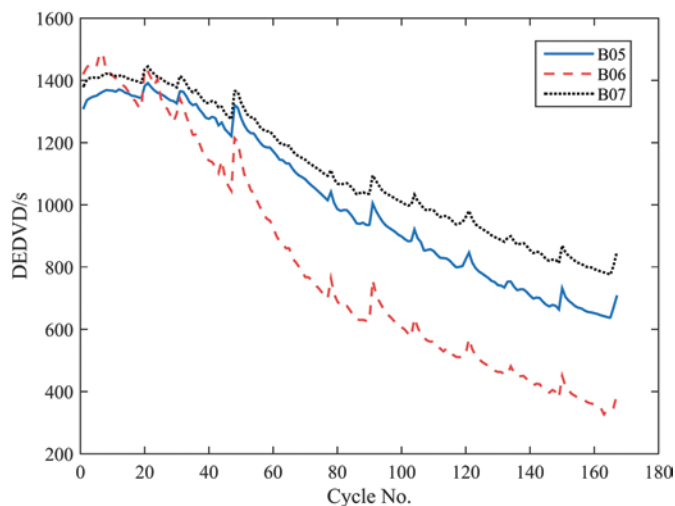


Fig. 6. Capacity degradation of tested batteries



(a) Variations of CR



(c) Variations of DTEDVD

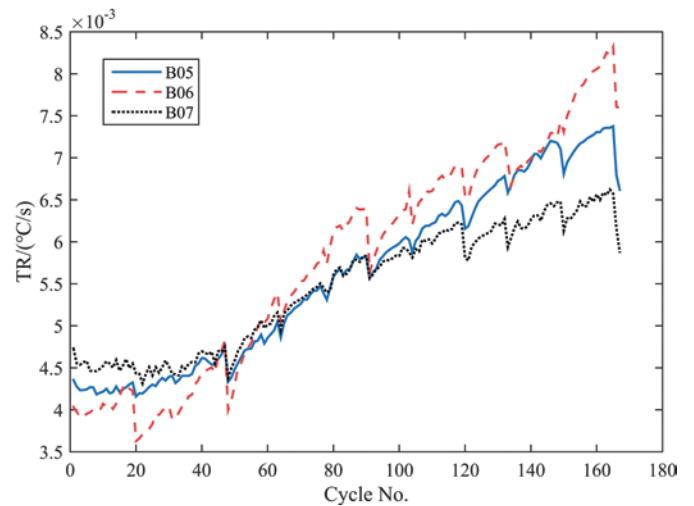
process, we calculate the HIs for batteries of B05, B06 and B07 respectively. Fig. 7 shows the variation of the four HIs with the increase of cycles respectively.

Next, we calculate the Pearson correlation coefficient between the four HIs and the original capacity of Li-ion batteries, as shown in Table 2. Obviously, the HIs have a close correlation with the capacity. Furthermore, the DTEDVD has a negative correlation with the capacity, while the other three HIs are in positive correlation.

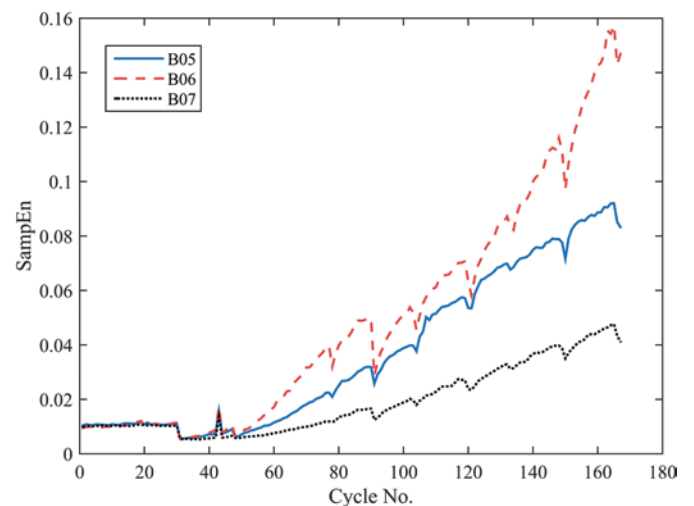
4.3. Establishing GRNN model

With the obtained HIs data, GRNN model is used to train and establish the mapping relationship between the HIs (input) and the capacity (output). In this study, the data of B05 and B06 batteries are used for training. On that basis, the well-trained GRNN model is used to estimate B07's capacity with B07's HIs. The predicted results are shown in Fig. 8.

As shown in Fig. 8, the proposed method has a relatively high prediction accuracy concerned with the capacity in the long-term trend. However, the predicted result is not so good for the first 40 points. The reason is that the HIs are not so stable during the early stage. Therefore, the first 40 points can be removed to obtain a more accurate prediction result.



(b) Variations of TR



(d) Variations of SampEn

Fig. 7. Variations of the four HIs changing with the charging cycles

4.2. Calculating HIs

In this section, by using the battery's historical operation data (including current, voltage and temperature) during the discharging

Moreover, the indicators, including root means square error (RMSE), the maximum estimation error and the maximum covariance (*cov*) value, are utilized to evaluate the accuracy of the estima-

Table 2. Correlation coefficient between HIs and capacity

Battery No.	B05	B06	B07
CR	-0.9791	-0.9893	-0.9658
TR	-0.9947	-0.9819	-0.9901
DTEDVD	0.9988	0.9957	0.9990
SampEn	-0.9522	-0.8936	-0.8876

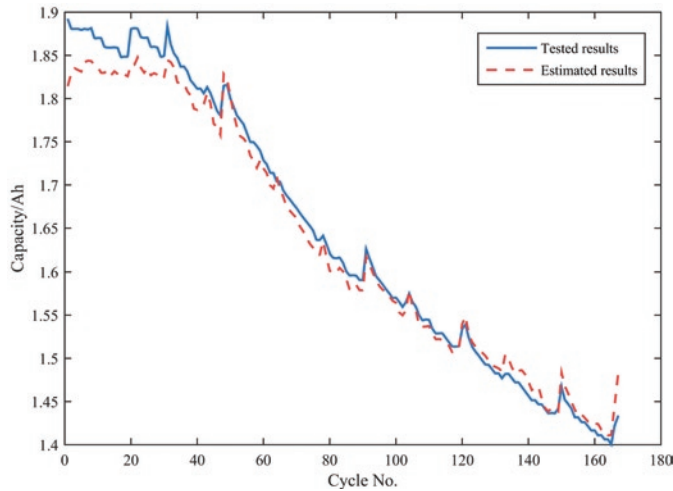


Fig. 8. The estimated and tested capacity of B07

Table 3. Accuracy analysis of the capacity estimation

Indicators	All points	Remove the first 40 points
RMSE	0.2002	0.0140
Max error	0.0823	0.0267
Max cov	0.0259	0.0110

tion results, as shown in Table 3. Obviously, the capacity estimation is with high accuracy.

4.4. RUL prediction

To remove the influence of self-regeneration phenomena and local fluctuations, a twice wavelet denoising is implemented with different thresholds. The result is shown as in Fig. 9.

In this case, the threshold of Sqtwolog method is larger than that of minimax method. As shown in Fig. 9, the first denoising can only eliminate the large noise signal, and the second denoising can elimi-

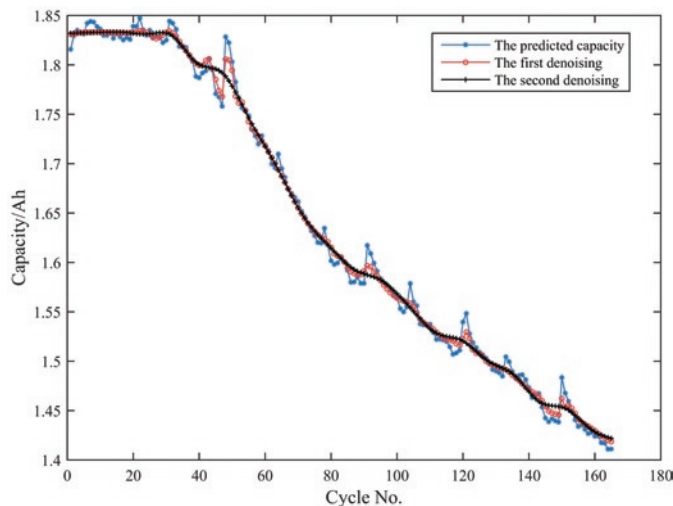
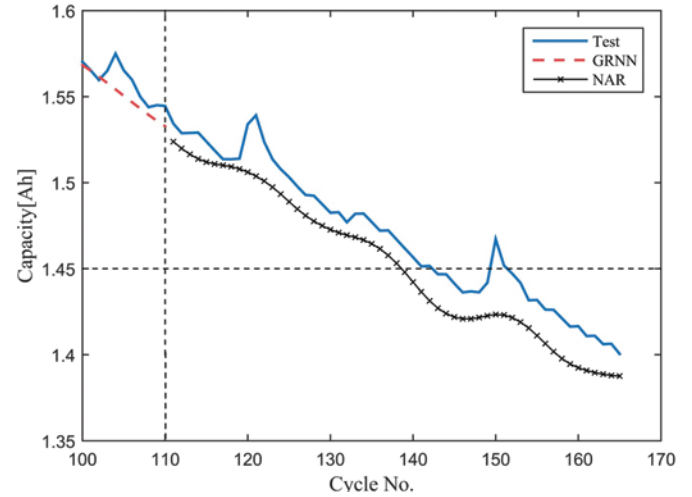


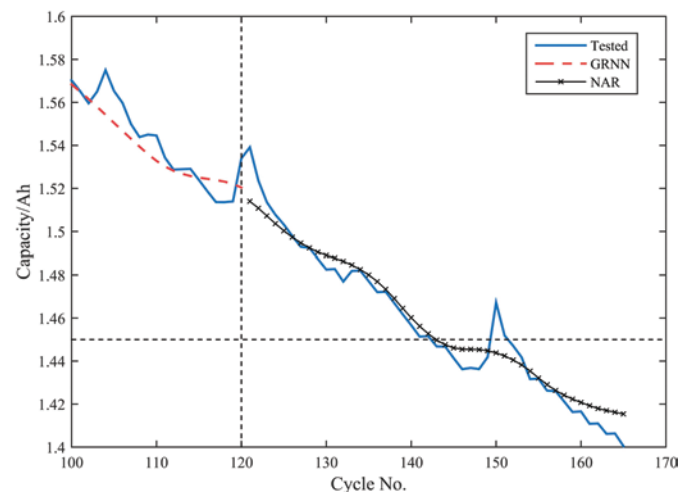
Fig. 9. The predicted capacity of B07

nate the smaller noise signal. Thus, with the proposed twice wavelet denoising, the noise can be eliminated more thoroughly and a more accurate prediction can be obtained.

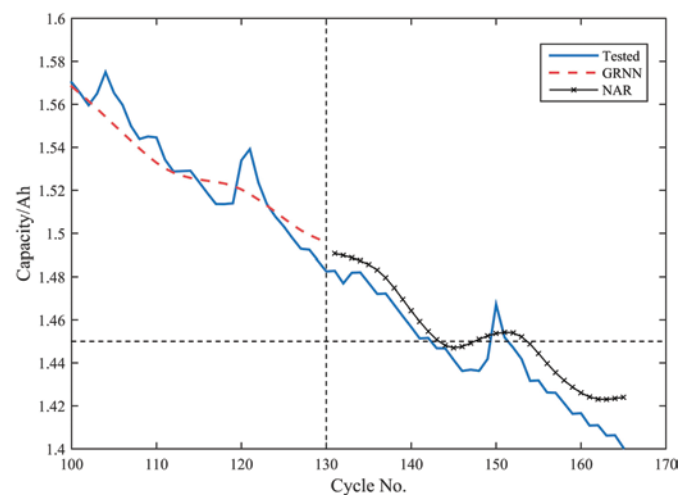
Based on the historical operation data, we can estimate the remaining capacity for each past cycle with the above steps. In addition, by selecting the obtained data points as the input set, the future degraded capacity can be predicted with the NAR model. On that basis, we can obtain the corresponding value of the RUL. Here, the number of the hidden layer is set as 1, the delay time is 20. It is supposed that the



M=110



M=120



M=130

Fig. 10. Predictions for B07's RUL under different M

Table 4. The predicted results of B07's RUL

M	Actual EOL	Actual RUL	Predicted RUL	Percentage Error/%
110	142	32	28	14.3
120	142	22	23	4.3
130	142	12	14	14.3

failure threshold of the battery capacity is 1.45Ah, and the total cycle life of B07 is 142. Here, we predict the B07's RUL when the operated cycles (M) are 110, 120, 130 respectively. In addition, considering that there is randomness in the training model, the predicted RUL will change with the experiments, thus we repeat the experiments for 100 times. Fig. 10 and Table 4 show some of the predicted results.

Set the range of the 100 predicted results as the RUL uncertainty bound (RUB). For the battery of B07, the RUB is shown as in Table 5.

Table 5. The RUB of B07 battery

M	Actual EOL	Actual RUL	RUB	Range
110	142	32	[28, 55]	27
120	142	22	[23, 45]	22
130	142	12	[14, 35]	21

With the above predicted results, we can conclude that the proposed methods can obtain the decline tendency of the Li-ion battery capacity with a high accuracy. However, the RUL's predicted result is not so stable. The possible reason is that the tested life cycle of the battery is not long enough. Therefore, the training data are not sufficient. Furthermore, considering that the capacity change during each cycle is too small, and a small error in capacity prediction may lead to a larger error in the RUL's prediction. It can also be found that the

Table 6. Predicted RUL results based on ARIMA model

M	Actual RUL	Predicted RUL	Error	Percentage Error/%
110	32	38	6	18.9
120	22	28	6	27.3
130	12	18	6	50.0

range of RUB will be narrowed down with the increase of the input cycles. It shows that the RUL prediction is sensitive to the number of input data. Therefore, by increasing the number of the training samples, the stability and robustness of the predictions can be improved.

References

- Chang Y, Fang H, Zhang Y. A new hybrid method for the prediction of the remaining useful life of a lithium-ion battery. *Applied Energy* 2017; 206: 1564–1578, <https://doi.org/10.1016/j.apenergy.2017.09.106>.
- Chen L, Xu L, Zhou Y. Novel approach for lithium-ion battery on-Line remaining useful life prediction based on permutation entropy. *Energies* 2018; 11(4): 820. <https://doi.org/10.3390/en11040820>.
- Donoho D L, Johnstone I M. Threshold selection for wavelet shrinkage of noisy data. *Proceedings of 16th Annual International Conference of the IEEE Engineering in Medicine and Biology Society* 1994; A24–A25, <https://doi.org/10.1109/iembs.1994.412133>.
- Donoho D L, Johnstone I M. Adapting to unknown smoothness via wavelet shrinkage. *Fundamental Papers in Wavelet Theory*. Princeton University Press 2014: 833–857, <https://doi.org/10.1515/9781400827268.833>.
- Feng J, Kvam P, Tang Y. Remaining useful lifetime prediction based on the damage-marker bivariate degradation model: A case study on lithium-ion batteries used in electric vehicles, *Engineering Failure Analysis* 2016; 70: 323–342, <http://dx.doi.org/10.1016/j.engfailanal.2016.04.014>.
- Hu X S, Li S, Peng H. A comparative study of equivalent circuit models for Li-ion batteries. *Journal of Power Sources* 2012; 198:359-367, <https://doi.org/10.1016/j.jpowsour.2011.10.013>.
- Hu X, Li S E, Jia Z, et al. Enhanced sample entropy-based health management of Li-ion battery for electrified vehicles. *Energy* 2014; 64: 953–960. <https://doi.org/10.1016/j.energy.2013.11.061>.
- Ibrahim M, Jemei S, Wimmer G, et al. Nonlinear autoregressive neural network in an energy management strategy for battery/ultra-capacitor

ARIMA model is also widely used in the battery's RUL prediction [21]. To compare the characteristics of different prediction models, here we make a comparison for RUL prediction with the ARIMA model. For the same input, the ARIMA method has a unique prediction result. Thus, the prediction results do not have a RUB. The RUL predicted results with ARIMA model are shown as in Table 6.

By comparing the three predicted results of different M , it can be found that for different M , the errors keep the same. It means that the prediction accuracy is not sensitive to the number of input cycles.

Comparing Table 4 and Table 6, it can be found that the predicted results of NAR model are more accurate than the results of ARIMA model. However, the predicted results are not as stable as the results of ARIMA model. Furthermore, since NAR model is sensitive to the number of the input data, the proposed NAR method is more suitable for large data set.

5. Conclusions

In this study, an innovative hybrid data-driven method is proposed to predict Li-ion battery's RUL, which is based on multiple HIs, including CR, TR, DTEDVD and SampEn. Furthermore, the GRNN model, NAR model and twice wavelet denoising are integrated. Case study shows that the proposed method can achieve Li-ion battery's RUL prediction with a high accuracy. Compared with ARIMA model, NAR model is more sensitive to the size of training samples. Meanwhile, the proposed method is established on the basis of battery historical data, it can overcome the limitation of online capacity measurement approaches. Moreover, the proposed RUL prediction method does not concern the physical and chemical reactions in the battery, thus it is well suitable for other kinds of batteries.

The future works can be focused on the following aspects: (1) to improve the robustness of the RUL prediction results, the NAR model can be improved further. (2) new HIs can be searched for more stable prediction, especially for the initial stage. (3) new RUL prediction methods can be developed by considering various operating environments of the Li-ion batteries.

Acknowledgement

This work is supported by the National Natural Science Foundation of China under No.71671035; the Open Fund of Hunan Provincial Key Laboratory of Health Maintenance for Mechanical Equipment, China under No.201901; Scientific Research Fund of Hunan Provincial Education Department, China under Grant No. 17A069, and the Open Fund of Jiangsu Wind Power Engineering Technology Center of China under ZK19-03-03.

- hybrid electrical vehicles. *Electric Power System Research* 2016; 136: 262–269, <https://doi.org/10.1016/j.epsr.2016.03.005>.
9. Kim I S. A technique for estimating the state of health of lithium batteries through a dual-sliding-mode observer. *IEEE Transactions on Power Electronics* 2009; 25(4): 1013–1022, <https://doi.org/10.1109/tpe.2009.2034966>.
 10. Kim J, Lee S, Cho B H. Complementary cooperation algorithm based on DEKF combined with pattern recognition for SOC/capacity estimation and SOH prediction. *IEEE Transactions on Power Electronics* 2011; 27(1):436–451, <https://doi.org/10.1109/tpe.2011.2158554>.
 11. Li Y, Wang K. Modified convolutional neural network with global average pooling for intelligent fault diagnosis of industrial gearbox. *Eksploracja i Niezawodność – Maintenance and Reliability* 2020; 22 (1): 63–72, <http://dx.doi.org/10.17531/ein.2020.1.8>.
 12. Liu D, Luo Y, Liu J, et al. Lithium-ion battery remaining useful life estimation based on fusion nonlinear degradation AR model and RPF algorithm. *Neural Computing and Applications* 2014; 25: 557–572, <https://doi.org/10.1007/s00521-013-1520-x>.
 13. Long B, Xian W, Jiang L, Liu Z. An improved autoregressive model by particle swarm optimization for prognostics of lithium-ion batteries. *Microelectronics Reliability* 2013; 53(6): 821–831, <https://doi.org/10.1016/j.microrel.2013.01.006>.
 14. Lyu C, Lai Q, Ge T, et al. A lead-acid battery's remaining useful life prediction by using electrochemical model in the particle filtering framework. *Energy* 2017; 120: 975–984, <https://doi.org/10.1016/j.energy.2016.12.004>.
 15. Patil M A, Tagade P, Hariharan K S, et al. A novel multistage support vector machine based approach for Li ion battery remaining useful life estimation. *Applied Energy* 2015; 159: 285–297, <https://doi.org/10.1016/j.apenergy.2015.08.119>.
 16. Prasad G K, Rahn C D. Model based identification of aging parameters in lithium ion batteries. *Journal of Power Sources* 2013; 232: 79–85, <https://doi.org/10.1016/j.jpowsour.2013.01.041>.
 17. Richman J S, Moorman J R. Physiological time-series analysis, using approximate entropy and sample entropy. *American Journal of Physiology-Heart and Circulatory Physiology* 2000; 278(6): H2039–H2049, <https://doi.org/10.1152/ajpheart.2000.278.6.h2039>.
 18. Saha B, Goebel K, Christophersen J. Comparison of prognostic algorithms for estimating remaining useful life of batteries. *Transactions of the Institute of Measurement and Control* 2009; 31: 293–308, <https://doi.org/10.1177/0142331208092030>.
 19. Saha B, Poll S, Goebel K, et al. An integrated approach to battery health monitoring using Bayesian regression and state estimation. *Proceedings of IEEE Autotestcon, 2007*; 646–653, <https://doi.org/10.1109/autest.2007.4374280>.
 20. Saha and B, Goebel K. Battery Data Set, NASA ames prognostics data repository. NASA Ames Research Center, 2007.
 21. Sbarufatti C, Corbetta M, Giglio M, et al. Adaptive prognosis of lithium-ion batteries based on the combination of particle filters and radial basis function neural networks. *Journal of Power Sources* 2017; 344: 128–140, <https://doi.org/10.1016/j.jpowsour.2017.01.105>.
 22. Song Y, Liu D, Yang C, et al. Data-driven hybrid remaining useful life estimation approach for spacecraft lithium-ion battery. *Microelectronics Reliability* 2017; 75: 142–153, <https://doi.org/10.1016/j.microrel.2017.06.045>.
 23. Su C, Chen H J. A review on prognostics approaches for remaining useful life of lithium-ion battery. *IOP Conference Series: Earth and Environmental Science* 2017; 93(1): 012040, <https://doi.org/10.1088/1755-1315/93/1/012040>.
 24. Valencia D, Orejuela D, Salazar J, et al. Comparison analysis between rigsure, sqtwolog, heursure and minimaxi techniques using hard and soft thresholding methods. *Proceedings of XXI Symposium on Signal Processing, Images and Artificial Vision (STSIVA) 2016*; 1–5, <https://doi.org/10.1109/STSIVA.2016.7743309>.
 25. Waag W, Kbitz S, Sauer D U. Experimental investigation of the lithium-ion battery impedance characteristic at various conditions and aging states and its influence on the application. *Applied Energy* 2013; 102: 885–897. <https://doi.org/10.1016/j.apenergy.2012.09.030>.
 26. Wei J, Dong G, Chen Z. Remaining useful life prediction and state of health diagnosis for lithium-ion batteries using particle filter and support vector regression. *IEEE Transactions on Industrial Electronics* 2017; 65(7): 5634–5643, <https://doi.org/10.1109/tie.2017.2782224>.
 27. Weng C, Cui Y, Sun J, et al. On-board state of health monitoring of lithium-ion batteries using incremental capacity analysis with support vector regression. *Journal of Power Sources* 2013; 235(4): 36–44, <https://doi.org/10.1016/j.jpowsour.2013.02.012>.
 28. Weng C, Sun J, Peng H. Model parametrization and adaptation based on the invariance of support vectors with applications to battery state-of-health monitoring. *IEEE Transactions on Vehicular Technology* 2015; 64(9): 3908–3917, <https://doi.org/10.1109/tvt.2014.2364554>.
 29. Widodo A, Shimb M C, Caesarendra W, et al. Intelligent prognostics for battery health monitoring based on sample entropy. *Expert Systems with Applications* 2011; 38(9): 11763–11769, <https://doi.org/10.1016/j.eswa.2011.03.063>.
 30. Wu J, Zhang C, Chen Z. An online method for lithium-ion battery remaining useful life estimation using importance sampling and neural networks. *Applied Energy* 2016; 173: 134–140, <https://doi.org/10.1016/j.apenergy.2016.04.057>.
 31. Xia Q, Wang Z, Ren Y, Sun B, et al. A reliability design method for a lithium-ion battery pack considering the thermal disequilibrium in electric vehicles. *Journal of Power Sources* 2018; 386:10–20, <https://doi.org/10.1016/j.jpowsour.2018.03.036>.
 32. Xia Q, Yang D, Wang Z, Ren Y, et al. Multiphysical modeling for life analysis of lithium-ion battery pack in electric vehicles. *Renewable and Sustainable Energy Reviews* 2020; 131: 109993, <https://doi.org/10.1016/j.rser.2020.109993>.
 33. Xing Y, Ma E W M, Tsui K L, et al. An ensemble model for predicting the remaining useful performance of lithium-ion batteries. *Microelectronics Reliability* 2013; 53(6): 811–820, <https://doi.org/10.1016/j.microrel.2012.12.003>.
 34. Yan S, Ma B, Zheng C. Health index extracting methodology for degradation modelling and prognosis of mechanical transmissions. *Eksploracja i Niezawodność – Maintenance and Reliability* 2019; 21 (1): 137–144, <http://dx.doi.org/10.17531/ein.2019.1.15>.
 35. Yu J, Yang J, Tang D, Dai J. Early prediction of remaining discharge time for lithium-ion batteries considering parameter correlation between discharge stages. *Eksploracja i Niezawodność – Maintenance and Reliability* 2019; 21 (1): 81–89, <http://dx.doi.org/10.17531/ein.2019.1.10>.
 36. Zhang C L, He Y G, Yuan L F, et al. Capacity prognostics of lithium-ion batteries using EMD denoising and multiple kernel RVM. *IEEE Access* 2017; 5: 12061–12070, <https://doi.org/10.1109/access.2017.2716353>.
 37. Zheng X, Fang H. An integrated unscented Kalman filter and relevance vector regression approach for lithium-ion battery remaining useful life and short-term capacity prediction. *Reliability Engineering & System Safety* 2015; 144: 74–82, <https://doi.org/10.1016/j.res.2015.07.013>.
 38. Zhou J, He Z, Gao M, et al. Battery state of health estimation using the generalized regression neural network. *Proceedings of 8th International Congress on Image and Signal Processing (CISP), 2015*; 1396–1400. <https://doi.org/10.1109/cisp.2015.7408101>.
 39. Zhou Y, Huang M. Lithium-ion batteries remaining useful life prediction based on a mixture of empirical mode decomposition and ARIMA model. *Microelectronics Reliability* 2016; 65: 265–273, <https://doi.org/10.1016/j.microrel.2016.07.151>.